


Analysis of a novel CuCl_2 back contact process for improved stability in CdTe solar cells

Elisa Artegiani^{1†} | Daniele Menossi^{1†} | Huw Shiel² | Vin Dhanak² | Jonathan D. Major² | Andrea Gasparotto³ | Kai Sun⁴ | Alessandro Romeo¹ 

¹LAPS—Laboratory for Photovoltaics and Solid State Physics, Department of Computer Science, University of Verona, Ca' Vignal 1, Strada Le Grazie 15, 37134 Verona, Italy

²Stephenson Institute for Renewable Energy and Department of Physics, University of Liverpool, Liverpool L69 7ZF, UK

³Department of Physics and Astronomy "G. Galilei", University of Padova, Via F. Marzolo 8, 35131 Padova, Italy

⁴Department of Materials Science and Engineering, University of Michigan, Ann Arbor, MI, USA

Correspondence

Alessandro Romeo, LAPS—Laboratory for Photovoltaics and Solid State Physics, Department of Computer Science, University of Verona, Ca' Vignal 1, Strada Le Grazie 15, 37134 Verona, Italy.
Email: alessandro.romeo@univr.it

Abstract

One of the crucial points in the production of CdTe solar cells is the insertion of copper in the back contact and in the absorber. As demonstrated by the top performing devices presented in literature: copper is necessary for high efficiency devices. However, despite this, copper was found to be a fast diffuser degrading the cell in the long term. Different approaches for limiting this effect have been widely presented from several laboratories, from the preparation of Cu_xTe by the controlled evaporation of Cu and Te to the application of ZnTe, which incorporates Cu, blocking its diffusion in the bulk. We have developed a wet deposition method for inserting in the CdTe structure a quantity of copper equivalent to a 0.1-nm-thick Cu layer. We are able to reach similar efficiencies to the ones of devices with a standard 2-nm-thick evaporated copper layer, but with a dramatic improvement in performance stability.

KEYWORDS

back contact, CdTe, copper, CuCl_2

1 | INTRODUCTION

CdTe and CIGS solar cells, with their respective records of 22.1% and 22.9%, have both reached efficiencies near to the 22.3% of multicrystalline silicon.¹

Thin film technology comprises ~5% of the world market, with CdTe modules accounting for around half of this.² Polycrystalline CdTe devices are partly limited by low doping concentrations, primarily due to the lack of a dopant with both high solubility and shallow acceptor level.³ One of the ongoing challenges of the technology is to produce a good quality and stable ohmic contact, because of the high CdTe electron affinity.⁴

The standard solution has been the insertion of copper at the back contact, which reduces the Schottky barrier via formation of $\text{Cu}_x\text{Te}_{1-x}$ phases and increased carrier concentration. This produces a "p⁺" layer at the near back surface which allows carriers to tunnel through the barrier.⁵ The mechanism of Cu doping for CdTe has been widely

studied^{6–8} and utilized in a variety of manners such as via simple copper evaporation or via inclusion in buffer layers at the back surface.^{9–13}

Whilst there has been some success with copper-free back contacts in the past, delivering efficiencies up to 15%,^{14,15} it is generally considered that copper is necessary to attain higher efficiency devices.

The use of copper in CdTe remains problematic however given it is a fast diffuser in CdTe and leads to performance degradation of the cells in the long term. Cu has previously been detected at the CdTe/CdS interface¹⁶ and at the CdS/CdTe junction forming recombination centres and shunt pathways.¹⁷ For this reason, different approaches have been applied to stabilize Cu at the back contact: such as the formation of Cu_xTe compounds by CdTe etching and subsequent Cu deposition,^{9,18} or the use of buffer layers such as As_2Te_3 ¹⁴ and Bi_2Te_3 ¹³ in order to avoid copper diffusion, or the development of a ZnTe:Cu back contact.¹⁹

In this paper, we analyse copper inclusion via a CuCl_2 -methanol solution. This process allows reduction of the incorporated copper quantity without any loss in performance compared with a standard Cu contacting route and simple depositing evenly over the entire area

[†]The first two authors share the same contribution to the work.

of the sample. Use of a chloride compound was chosen due to the well-known chlorine-related benefits of recrystallization, grain growth,²⁰⁻²² and p-type doping (bicomplexes with native defects)^{20,23} in CdTe. There is evidence that similar processes have been already applied in some laboratories but without a study of the process' effect.²⁴⁻²⁸

Beach et al suggested that the defects induced by CdCl₂, probably Cl-induced donor, increased the solubility of the Cu at Cd substitutional sites impurities Cu⁻_{Cd}, which are considered acceptors.²⁹

The CuCl₂ is applied after the standard CdCl₂ activation treatment because combining activation treatment and copper doping in a single step is not possible: CdCl₂ activation treatment is applied at a temperature which would cause a very large Cu diffusion.

The results of this copper chloride wet deposition method (CCWD) on CdTe are the following:

- i. Less Cu required to achieve peak performance: with amount of copper solution which is the equivalent of a 0.1-nm-thick evaporated layer, JV characteristic shows a good ohmic back contact without roll over.
- ii. Scalable deposition process where copper content can be easily controlled by tuning its concentration in methanol solution.
- iii. Improved stability: proved by accelerated aging tests performed at an illumination of one sun and at a temperature of 80°C.

2 | MATERIALS AND INSTRUMENTS

Current density-voltage (JV) characteristics were measured with a Keithley Source Meter 2420, using a halogen lamp calibrated with a silicon solar cell under an irradiation of 100 mW/cm² (AM 1.5).

Drive level capacitance profiling (DLCP), capacitance voltage (CV), and admittance spectroscopy (AS) are carried out by a HP4284A LCR. The temperature is controlled by a Janis cryostat with Lakeshore 325 temperature controller in a vacuum of 10⁻⁴ Pa and in a range between 100 and 320 K.

The external quantum efficiency (EQE) was obtained using a commercial LOANA solar cell analysis system, calibrated with a silicon reference sample with known EQE using an incident spotlight of 1 mm × 2 mm area.

The crystalline structure and the compositional phases were analysed by X-ray diffraction (XRD) with a Philips vertical diffractometer with Cu-K α radiation and Goebel monochromator.

Secondary ion mass spectrometry (SIMS) depth profiles were obtained on a CAMECA IMS-4 f using an O₂⁺ primary ion beam at a 12.5-kV accelerating voltage (corresponding to 8-keV impact energy) and detection of positive secondary ions. A mass resolution $m/\Delta m \approx 4000$ was employed in the spectrometer to avoid mass interference between the ⁶³Cu⁺ and the ¹²⁶Te⁺ signals.

X-ray photoelectron spectroscopy (XPS) experiments were performed in a standard ultrahigh vacuum surface science chamber operating at a base pressure of 2×10^{-10} mbar. Core-level electronic structure was probed using a dual anode Mg K α (1253.6 eV) X-ray source operating at 200 W and a hemispherical PSP Vacuum Technology electron

energy analyser. The spectrometer was calibrated using Au 4f_{7/2} at 83.9 eV and has an overall resolution of 0.7 eV. XPS spectra were fitted using Voigt functions after Shirley background removal.

For tunnelling, electron microscopy-energy dispersive X-ray (TEM-EDX) analysis a JEOL 2100F microscope with CEOS probe corrector was used that was operated in scanning transmission electron microscopy (STEM) mode to acquire simultaneous high angle annular dark-field (HAADF) images, ie, Z-contrast images, together with EDX element maps. A focused ion beam (FIB) in-situ lift-out method was used for cross-sectional TEM specimen preparation. The CdTe morphology was characterized by NT-MDT Solver Pro atomic force microscopy (AFM) in semi-contact mode and NSG-01 silicon tip.

3 | DEVICE FABRICATION

CdTe thin film solar cells are made in superstrate configuration by a low-temperature fabrication process based on vacuum evaporation (VE). A 100-nm-thick CdS thin film is deposited at 150°C on an ITO/ZnO 3 × 3 cm² coated soda lime glass and subsequently annealed in vacuum at 450°C. Then, a 7- μ m-thick CdTe layer is deposited in the same vacuum chamber. The stack is activated by the CdCl₂ treatment, consisting of deposition which is applied by wet deposition, and annealed in air at 380°C.

Prior to the back contact deposition, the CdTe surface is etched by a bromine/methanol solution in order to remove CdCl₂ residues and to generate a Te-enriched layer and allow the formation of a Cu_xTe compound.

In our standard process, back contact is made by thermal evaporation of a 2.0-nm-thick copper layer followed by a 30-nm-thick gold layer; annealing in air at 200°C of the finished device is needed to reach good efficiencies.

The CCWD process for CdTe consists of depositing on top of the CdTe layer a solution made of CuCl₂ powder diluted in methanol, typically 0.1 g of CuCl₂ per litre of methanol. An annealing of the stack at 200°C for 30 minutes is applied to allow a chemical reaction between the bulk and the solution. Finally, a 30-nm-thick gold contact is deposited on free back surface. In order to compare the CCWD with the VE process, we have deposited on top of the CdTe surface an amount of CuCl₂ solution, which is equivalent to a copper layer with a thickness of 0.1 nm. This has been calculated by comparing the amount of copper in the laid out solution with the value obtained by multiplying the copper volume of the thin evaporated layer by its density.

Practically 0.4726 μ g of copper has been deposited on an area of 4.5 cm² of a 7- μ m-thick CdTe. Calculating the amount of copper atoms from its atomic mass, we have about 1×10^{15} atoms/cm² near to the 0.8×10^{15} atoms/cm² indicated by Kranz et al.⁸

4 | RESULTS

4.1 | Performance of the devices

A large number of samples have been fabricated with the CCWD step process, where the amount of used solution ranged from 10 to 20 μ L

(pure methanol is also added to improve uniformity) while annealing temperature was optimized at 200°C. Also, optimization of both CdCl₂ treatment and CCWD step were done together in order to achieve the best combination in terms of performance. In this way, more than 50 samples, with 10 solar cells each of 0.13 cm², were produced with the new step process.

These devices have been compared with samples using either a 2 or 0.1-nm VE-Cu contacting process. This last one has a very similar copper quantity of the CCWD cells but deposited by VE and without chlorine. In order to avoid the performance degradation effects due to copper diffusion, one option could be to minimize the amount of copper applied, but this would reduce the performance, due to lower CdTe doping and to a higher back contact barrier.

Figure 1 shows J-V characteristics of three of our best devices obtained inserting copper by evaporation and by wet deposition. Clearly, reducing the amount of evaporated copper from 2 to 0.1 nm, the conversion efficiencies reduce as expected (see Table 1). The reduction is mainly caused by a fill factor (FF) loss concurrent to a pronounced rollover.

On the other hand, if the equivalent of a 0.1-nm-thick copper layer is inserted by CCWD on the CdTe, the series resistance is reduced and FF largely increases and conversion efficiencies are comparable to the ones of devices with a 2-nm-thick back contact layer.

This is quite interesting because it proves that a very small amount of copper (see Section 3) is sufficient for CdTe doping as reported by Kranz et al.⁸ However, it is very important how and where the Cu is

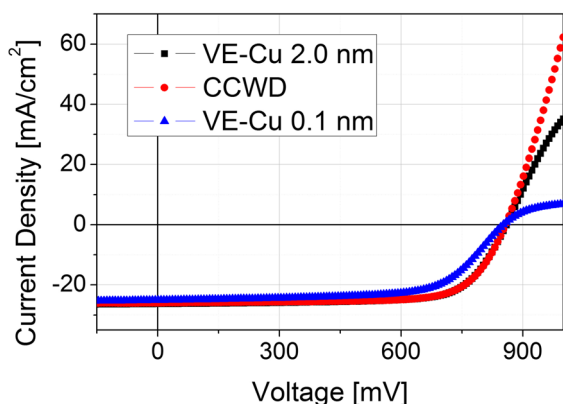


FIGURE 1 Comparison between J-V characteristics of devices with 2.0 and 0.1-nm-thick copper layer by evaporation (respectively, black and blue), and with the equivalent amount of a 0.1-nm-thick copper layer by wet deposition (red) [Colour figure can be viewed at wileyonlinelibrary.com]

TABLE 1 Efficiency parameters of devices of Figure 1: Conversion efficiency (η), fill factor (FF), open circuit voltage (V_{oc}), and short circuit current density (J_{sc})

Copper Quantity	η , %	FF, %	V_{oc} , mV	J_{sc} , mA/cm ²
CCWD	15.9 ± 0.2	73.1 ± 0.5	859 ± 1	25.4 ± 0.1
VE-Cu 2.0 nm	16.1 ± 0.2	72.0 ± 0.5	866 ± 1	25.8 ± 0.1
VE-Cu 0.1 nm	13.8 ± 0.2	66.0 ± 0.5	852 ± 1	24.5 ± 0.1

blended in the CdTe matrix, avoiding agglomeration at grain boundaries.

Looking at Table 2, the average performance parameters show that samples containing a 0.1-nm-thick copper layer deposited by CCWD reach almost the same average efficiency (η) than samples containing a 2.0-nm-thick copper layer deposited by VE (VE-Cu). In particular, the average FF of CCWD samples is slightly larger which is quite surprising considering the small amount of Cu.

The choice of CuCl₂ as Cu carrier has been done according to the well-known effects of chlorine-based treatments, enhancing a chemical reaction with CdTe,³⁰ generating a rearrangement of the CdTe structure and reducing the grain boundaries' effect. However, the results show that inserting copper by chlorine carrier improves the back contact, but it cannot be excluded that it also might change the interface and the bulk structure of the absorber.

In order to clarify this aspect, an analysis of the spectral response of two different cells, with efficiencies around 13%, has been pursued by EQE measurements, performed on CCWD and VE-Cu samples. EQE responses of the different cells do not show significant differences, attesting that CCWD does not influence band gap or carrier lifetime. Similar response for different cells at long-wavelength region shows that the CdS_xTe_{1-x} intermixed layer has not been modified by the additional chlorine treatment; as it is known that the formation of an intermixed layer reduces the band gap,³¹ shifting the EQE response.

4.2 | Structural analysis

The activation treatment, with CdCl₂, is typically changing the grain structure of the absorber, in particular is affecting both shape (and size in case of low temperature deposited CdTe) and orientation of the grains.³²

Thus, it is interesting to verify if the CCWD process would also modify the structure of the CdTe bulk, due to the presence of chlorine. For this reason, XRD patterns have been acquired on the surface of the completed VE-Cu and CCWD photovoltaic devices (see Figure 2), considering that in the standard geometry, the X-rays are able to penetrate more than 0.5 μ m in the stack.

As shown in Figure 2, CdTe peaks are present in both samples, as expected.

Moreover, we can observe a slightly different recrystallization for the CCWD case, where the preferential orientation of the (111) peak is completely lost in favour of the (422) orientation. In particular, for the VE-Cu case, (111) > (311) and (442) while for the CCWD case (442) > (311) > (111). This shows that copper chlorine introduces

TABLE 2 Average efficiency parameters of devices

Copper Quantity	η , %	FF, %	V_{oc} , mV	J_{sc} , mA/cm ²
CCWD	15.7 ± 0.3	71.4 ± 1.4	852 ± 5	25.8 ± 0.3
VE-Cu 2.0 nm	15.9 ± 0.1	71 ± 1.3	852 ± 10	26.4 ± 0.7
VE-Cu 0.1 nm	13.8 ± 0.2	66.2 ± 0.8	847 ± 2	24.6 ± 0.5

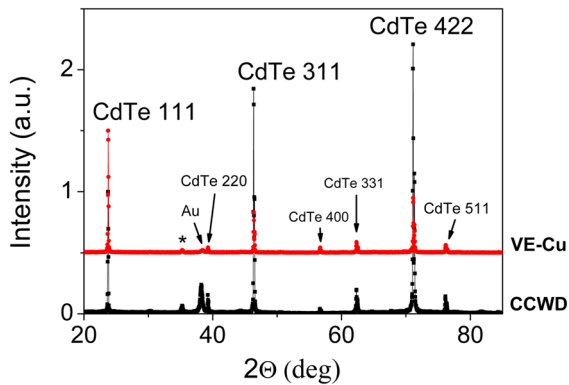


FIGURE 2 XRD spectra of VE-Cu and CCWD finished devices [Colour figure can be viewed at wileyonlinelibrary.com]

copper in the bulk of CdTe by changing its structure, affecting the orientation of the grains. Also, AFM pictures show a slightly different grain structure, as depicted in Figure 3.

4.3 | Doping and identification of defects

A very important aspect is understanding the effects of the different copper insertion processes in the CdTe doping. As already mentioned, a reduced Cu quantity would suggest a lower CdTe doping, but this appears to be in contrast with the devices performances, which in the case of CCWD samples does not suffer of any Cu deficiency. With capacitance voltage (CV) and drive level capacitance profiling (DLCP) measurements on VE-Cu and CCWD samples, the net charge density in CdTe of acceptor-minus-donor states can be estimated as a function of distance from the junction. The CV profiles (indicated in Figure 4 with open dots) show the contribution of both deep and shallow defects, while the deepest states hardly affect the DLCP curves

(full dots), so the difference between each pair of curves is associated to the presence of deep states.³³

At 1 MHz, the net charge density profile of the VE-Cu sample (see Figure 4, graph on the right) is much more temperature dependent than the CuCl₂ one: as the temperature rises, in the VE-Cu case (Figure 4, right side), the net charge density increases constantly with temperature, while in CCWD case (Figure 4 left side) the main increase happens only between 240 and 270 K. This suggests that the dominant defects are of different nature in the two samples, though both types of samples show the presence of deep defects. The net charge density is determined from the lower part of the U-shape profile in order to avoid effects due to others factors, such as a not perfectly ohmic back contact or the limited thickness of CdTe.³⁴ At 300 K, the VE-Cu sample shows a little higher net charge density than the CCWD case: $2 \times 10^{14} \text{ cm}^{-3}$ versus $1.5 \times 10^{14} \text{ cm}^{-3}$. At 210 K, the net charge density of the VE-Cu sample drops at $3 \times 10^{13} \text{ cm}^{-3}$ while it stays at $6 \times 10^{14} \text{ cm}^{-3}$ for the CCWD case; in the first case, we can conclude that some defects freeze out. Again, in Figure 4, the profiles referred to the VE-Cu case increase in the right part of the graph; this effect is influenced by the back contact, revealing that the depletion region extends too close to the contact.

Similar analysis has been done also at lower frequencies such as 10 kHz (see Figure 5): in the VE-Cu case, we can imagine that some defects are slower and/or more distant from the valence band³³ compared with that of the CCWD case. The defects in the VE-Cu type are following the voltage signal at high temperature or at low frequency: so that at 10 kHz, the net charge density is $3 \times 10^{14} \text{ cm}^{-3}$. On the other hand, for the CCWD sample, the net charge density stays stable at $1.5 \times 10^{14} \text{ cm}^{-3}$.

Because the samples, except for the copper deposition step, have similar fabrication process, we can conclude that the CuCl₂ treatment results to different defects in the CdTe.

However, the overall net charge density is very close for the two processes. Thus, it can be concluded that CdTe has similar level of

FIGURE 3 Morphology of CdTe before (left) and after (right) CCWD treatment process [Colour figure can be viewed at wileyonlinelibrary.com]

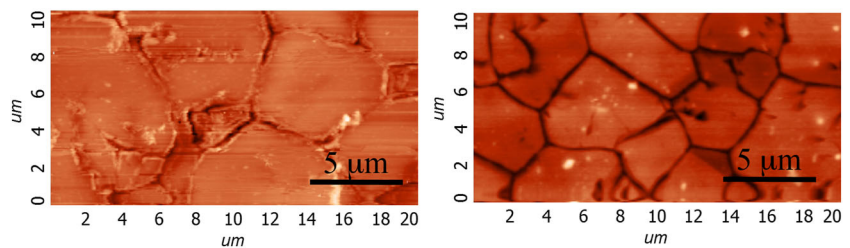
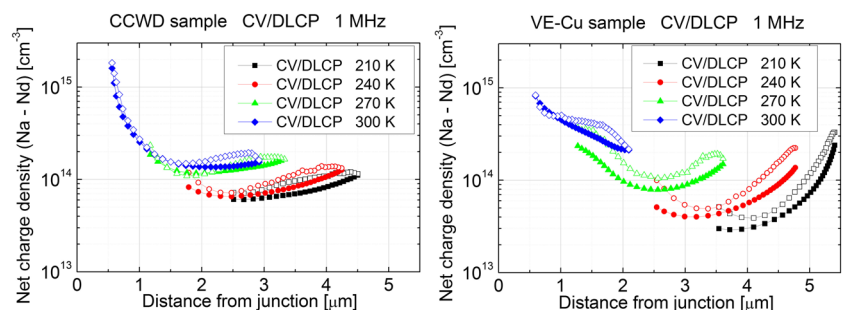


FIGURE 4 Comparison between CV (open dots) and DLCP (full dots) measurements of a CCWD sample (left) and a Cu sample (right) at 1 MHz [Colour figure can be viewed at wileyonlinelibrary.com]



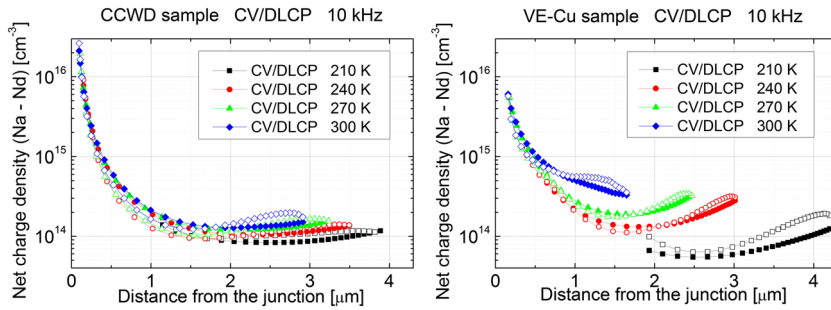


FIGURE 5 Comparison between CV (open dots) and DLCP (full dots) measurements of a CCWD sample (left) and a Cu sample (right) at 10 kHz [Colour figure can be viewed at wileyonlinelibrary.com]

doping with a reduced amount of Cu, if introduced with chlorine carrier, compared with the 2-nm-thick copper layer deposited by evaporation.

In order to identify the nature of the different defects seen by CV-DLCP measurements and to understand what happens when copper is introduced in CdTe bounded to chlorine, admittance spectroscopy analysis was performed on VE-Cu and CuCl_2 samples. AS measurements allow to estimate the activation energy (E_a) and cross section (σ_a) of the dominant traps above the valence band and identify the nature of the defects (see Figure 6 and Table 3).

Both samples show the presence of defect A, identified as the $\text{V}_{\text{Cd}}\text{-Cl}_{\text{Te}}$ complex, usually called A centre.²³ However, they show also different deep defects: in the CuCl_2 sample, two defects (B) are detected: with E_a between 0.34 and 0.37 eV above the valence band. In this

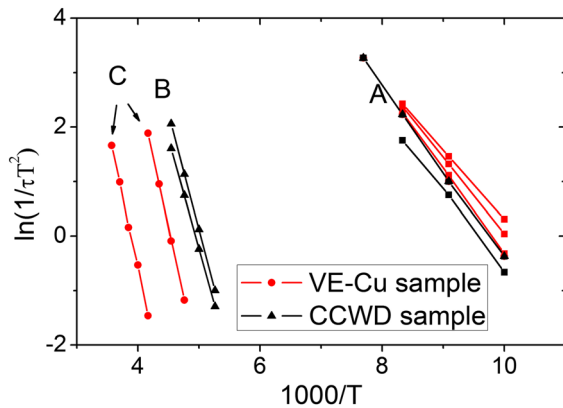


FIGURE 6 Arrhenius plot of the admittance spectroscopy data obtained from VE-Cu and CCWD samples [Colour figure can be viewed at wileyonlinelibrary.com]

TABLE 3 List of defects identified by admittance spectroscopy

CCWD Sample		Attribution	VE-Cu Sample	
E_a , meV	σ_a , cm^{-2}		E_a , meV	σ_a , cm^{-2}
		A	109 ± 3	1.9×10^{-16}
125 ± 6	4.6×10^{-16}	A	121 ± 4	5.5×10^{-16}
136 ± 4	2.0×10^{-15}	A	134 ± 3	1.7×10^{-15}
349 ± 5	2.0×10^{-13}	B		
367 ± 6	8.2×10^{-13}	B		
		C	445 ± 10	5.8×10^{-12}
		C	449 ± 9	1.9×10^{-13}

range, the defects are attributed to the Cu at Cd substitutional sites impurities $\text{Cu}_{\text{Cd}}^{-}$.^{29,35} These were also detected by Beach et al: they reported that the concentration of these defects was higher in CdCl_2 -treated samples, implying that the defects induced by CdCl_2 (probably Cl-induced donor) increased the solubility of $\text{Cu}_{\text{Cd}}^{-}$.²⁹

In this paper, all the samples are CdCl_2 treated; however, by detecting these defects only for the CuCl_2 sample suggests that Cl presence increases the Cu solubility into the CdTe bulk. Moreover, by reducing the amount of copper the number of interstitial copper defects, Cu_i is also reduced.

It has been reported that the Cu substitution in Cd vacancy $\text{Cu}_{\text{Cd}}^{-}$ acts as an acceptor, by increasing the p-type doping, while the interstitial copper Cu_i is a shallow donor, which compensates the doping.^{29,35,36} For this reason, the formation of the $\text{Cu}_{\text{Cd}}^{-}$ defects is desirable.

On the other hand, $\text{Cu}_{\text{Cd}}^{-}$ levels are not measured in the VE-Cu sample, despite the higher copper concentration. However, this shows that this type of defect is not dominant in the VE-Cu sample. In this case, due to the large amount of copper, $\text{Cu}_{\text{Cd}}^{-}$ and Cu_i are compensated.

The VE-Cu sample shows two deeper dominant defects (C) in the range of 0.43 to 0.45 eV above the valence band, usually detected in our standard samples,^{18,37} which are not clearly attributed. Beach et al²⁹ as well as Wei et al³⁸ consider plausible to assign these values to the U-centre Te^{2-}_i ; a deep acceptor level. Also, Beach et al highlight that these defects have a higher density for CdCl_2 -treated samples, implying that CdCl_2 contributes to their formation; this has been previously observed also in our samples.³⁷

4.4 | Analysis of the diffusion of copper element

Figure 7 shows HAADF images together with corresponding EDX Cu maps on CuCl_2 and VE-Cu devices. The two EDX maps are not normalized, and for this reason they cannot be compared in absolute values (ie, signal intensity); however, our aim here is to analyse the distribution of the copper in each sample.

In both samples, copper is distributed throughout the CdTe layer, including the back contact region. Nevertheless, in the picture for the first case, the magenta colour is almost homogeneously distributed while for the second case it is concentrated at the back. This means a larger uniformity of copper for the VE-Cu case (top), as a larger content of magenta colour is observable all over the CdTe bulk. On the

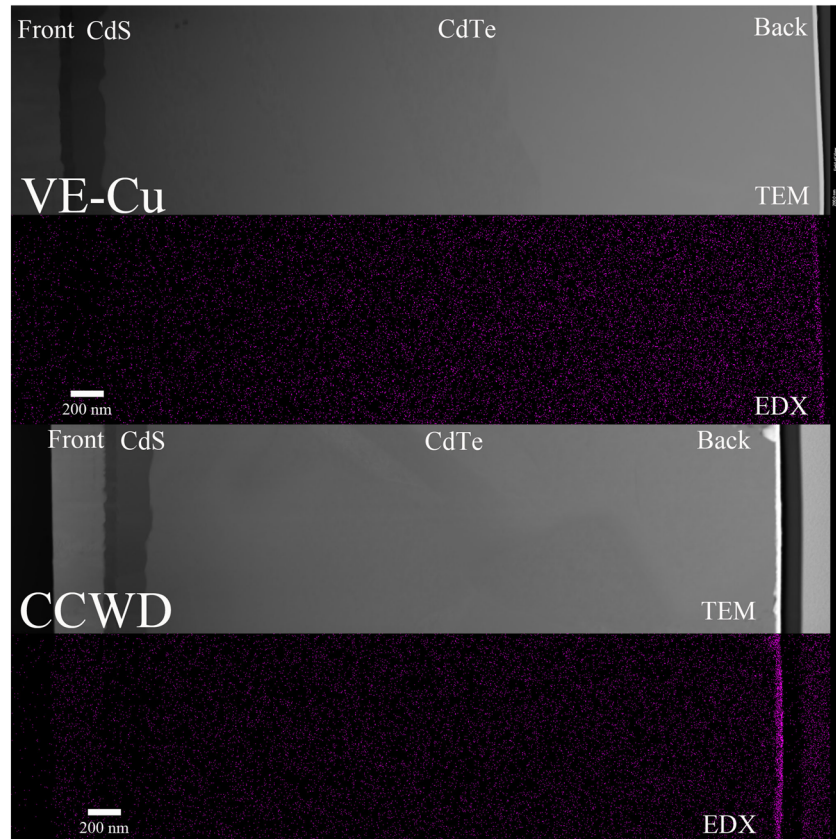


FIGURE 7 Comparison between HAADF images and corresponding EDX Cu maps of VE-Cu (top) and CCWD sample (bottom) [Colour figure can be viewed at wileyonlinelibrary.com]

other hand, the CCWD case shows a strong difference in the copper distribution: a higher contrast is observed near the back contact.

This suggests that in the CuCl_2 sample a larger amount of copper is fixed at the back contact despite it is 1/20 of the evaporated copper (see Section 3). The fact that most of the copper is kept at the contact explains the lower back contact barrier in the CuCl_2 sample and so the high FF value.

In order to check and confirm this observed different rate of copper diffusion, SIMS depth profiles have been analysed in the VE-Cu and the CCWD samples; both samples were coated with a 25-nm-thick gold layer.

The SIMS profiles (shown in Figure 8) confirm the highest amount of copper on the surface for the VE-Cu case. The Cu, in this case, diffuses into the gold layer, so near the surface a large amount of Cu is registered. So when we have to compare the two different samples,

for VE-Cu, we should consider the amount measured at a depth of 30 nm, value where the copper presence starts in the CCWD sample.

Moreover, in the VE-Cu sample, there is a large copper diffusion in the first 400 nm (in depth); over this value, the signal reduces at the limit of the sensitivity of the instrument. For the CCWD sample, the signal decreases to the sensitivity limit within 200 nm; moreover, the copper amount in this region is lower than in the VE-Cu sample. Finally, in the VE-Cu sample, we can observe copper diffusion inside the gold layer, due to the annealing of the finished back contact.

4.5 | Back surface analysis

Although the copper distribution in the CdTe varied dependent on the application method, it is useful to determine if it stays in elemental

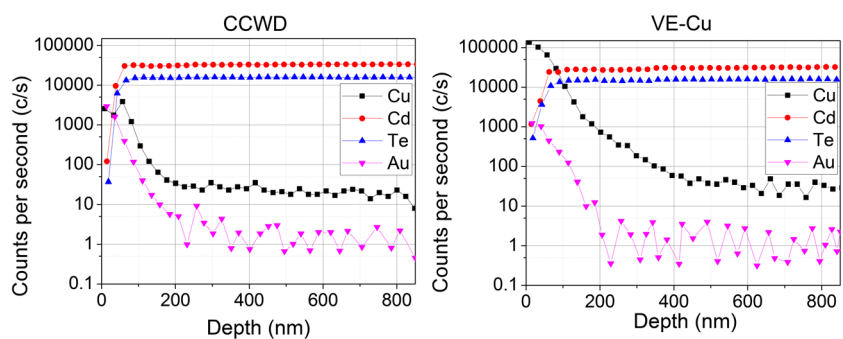


FIGURE 8 SIMS depth profiles of CCWD (left) and VE-Cu (right) finished devices [Colour figure can be viewed at wileyonlinelibrary.com]

form or if it generates different compounds on the CdTe surface. For this purpose XPS characterization has been performed on the surface of VE-Cu and CCWD samples; both samples were prepared with only 5-nm-thick gold layer on top, in order to allow the analysis.

In Figure 9, the XPS Te 3d core levels show that while in the CuCl₂ sample Te-O and Te/Te-Cd peaks have comparable heights; in the VE-Cu sample, the Te-O peaks are much more intense than the Te/Te-Cd ones. Jun-Feng et al.³⁹ reported a same increase of the Te-O peak and decrease of the Te/Te-Cd peak when leaving the CdTe sample exposed to air. So, we can conclude that in the VE-Cu sample, the Te layer is mainly oxidized, while for the CCWD case Te-O and elemental Te/Te-Cd have similar signals; thus, the CCWD sample shows a larger presence of Te in the back contact region. This can explain the improved performance of the back contact for CCWD case (no roll-over in the J-V curve is observed). A Te layer is widely used as a buffer to improve the back contact because of its high valence band maximum, which is around 5.40 to 5.45 eV and stays at intermediate levels between the CdTe valence-band maximum (5.8 eV) below the vacuum level and the gold work function (5.1 eV). It reduces the CdTe back contact barrier.⁴⁰

Very important is that despite the lower Cu amount for the CCWD case, this sample shows high Te-Cd peaks. Thus, in this case, at the back contact it is placed a larger amount of copper (as supported by the already shown EDX mapping during TEM analysis). Moreover, an XPS study on Cu-free CdTe was made for reference. The change in separation between the two main peaks (Te-Cd and Te-O bonding) supports the presence of the Te-Cu component.

From this analysis, we can conclude that depositing CuCl₂ on a Te rich layer (generated by the Br-MeOH etching), the Te binds with Cu during the annealing step oxidizing to a very limited extent. This is

another part of the jigsaw that explains the higher performance of the back contact, because Cu_xTe buffer binds Cu and reduces its diffusion in the bulk as shown by Wu et al.⁹ This buffer can also be generated by depositing copper on the bromine-methanol etched CdTe surface as shown by Rimmaudo et al.¹⁸

5 | DISCUSSION AND PERFORMANCE STABILITY OF THE CELLS

At this stage, we have acquired that the CuCl₂ step process is able to provide a performing back contact with a minimum amount of copper.

XPS, SIMS, and EDX analyses confirm that a large amount of Cu is concentrated and fixed very near to the back contact suggesting a superior stability of the finished devices.

The best way to analyse and verify the performance degradation of the solar cells according to the different process discussed here is to apply accelerated stress tests (AST) on the photovoltaic devices. In a specific metal chamber, where a rack of halogen lamps and a temperature-controlled system allows to keep the cells under an

TABLE 4 Average efficiency parameters of CuCl₂ and VE-Cu devices before the aging, and after 1008 h of AST

Samples	η , %	FF, %	Voc, mV	Jsc, mA/cm ²
CuCl ₂ before aging	13.9 ± 0.3	67 ± 2	845 ± 3	24.5 ± 0.4
CuCl ₂ after 1008 h of AST	10.6 ± 0.4	57 ± 3	764 ± 4	24.2 ± 0.4
VE-Cu before aging	13.9 ± 0.8	69 ± 4	849 ± 5	23.6 ± 0.2
VE-Cu after 1008 h of AST	7.3 ± 0.4	47 ± 2	694 ± 5	22 ± 1

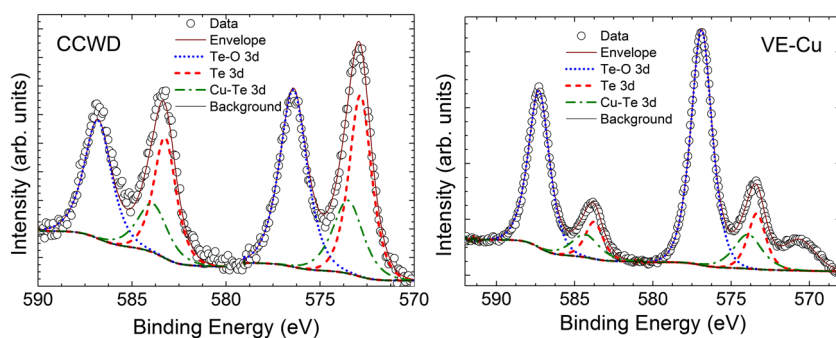


FIGURE 9 XPS spectra of finished CCWD (left) and VE-Cu devices (right) are shown, tantalum is used for contacting the cells [Colour figure can be viewed at wileyonlinelibrary.com]

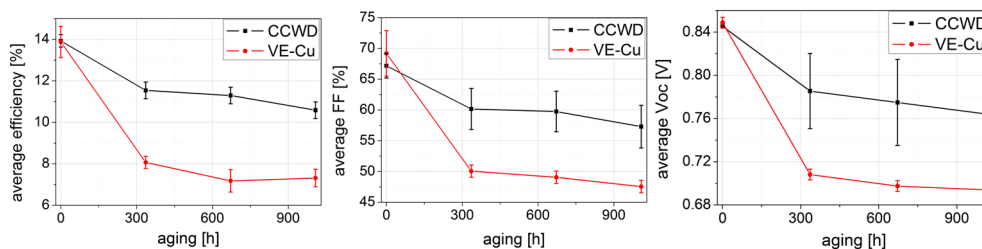


FIGURE 10 Graph reporting the performance degradation along time of the Cu and CuCl₂ samples. Results concerned to average efficiency on the left, to average FF in the centre, and to average Voc on the right are, respectively, displayed [Colour figure can be viewed at wileyonlinelibrary.com]

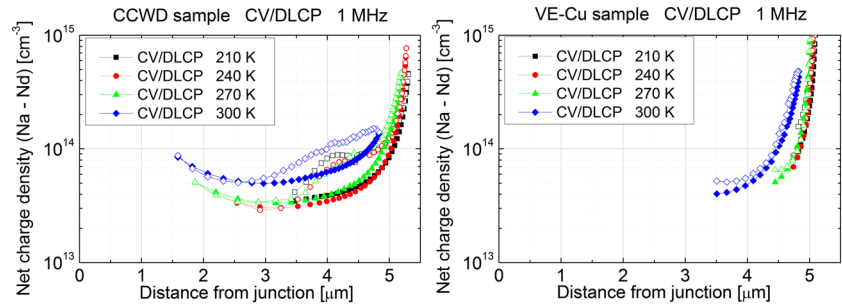


FIGURE 11 Comparison between CV (open dots) and DLCP (full dots) measurements of CuCl_2 sample (left) and Cu sample (right) after 336-h AST [Colour figure can be viewed at wileyonlinelibrary.com]

illumination of around 1000 W/m^2 and at a temperature of 80°C , the cells are positioned for a time up to 1000 hours and their conversion efficiency measured every 300 hours.

Two different sets of solar cells were positioned in the AST box, one with VE-Cu samples and one with CCWD samples; both exhibited an average efficiency of about 14% prior to aging. Their performance degradation has been analysed by measuring their efficiencies at different time steps.

As it can be seen in the graph on the left of Figure 10 and on Table 4, the CCWD samples show a reduced degradation. In particular, after 1008 hours of aging, they have an average efficiency of $(10.6 \pm 0.4) \%$ compared with the $(7.3 \pm 0.4) \%$ of the Cu samples. The cells show their major efficiency drop during the first period of aging, and also just after 336 hours the average efficiency discrepancy is clear: $(11.5 \pm 0.4) \%$ versus $(8.1 \pm 0.3) \%$.

The different level of degradation depends mainly on the FF: after 1008 hours, setting to 100 the initial values, the average FF of CCWD samples is reduced to 85% of its initial value, the average V_{oc} to 90%, and the average J_{sc} to 99%. On the contrary, the VE-Cu samples have reduced their average FF to 69%, their average V_{oc} to 82%, and their average J_{sc} to 95%.

After the complete AST cycle, the CCWD samples exhibit 76% of the initial average conversion efficiency, while the efficiencies of the VE-Cu samples are halved.

The higher stability of CCWD-CdTe devices compared with the VE-Cu ones, as expected from the characterizations that have been discussed above, is confirmed. The extremely reduced amount of Cu (more than 20 times less) in the CCWD device also contributes to this stability. Diffusion is proportional to concentration, the amount of Cu which diffuses into the CdTe layer is regulated by its concentration gradient in the absorber film.

When large Cu amount is diffused, it can lead to shunt paths, reflecting in reduced FF as observed in this paper. So, according to this argument, more Cu delivers increased migration towards the p-n junction. This hypothesis has been also partly confirmed by additional CV-DLCP characterizations, which were made on VE-Cu and CCWD samples after 336-hour AST, where the main drop in efficiency value is occurred.

By comparing these profiles (shown in Figure 11) with the pre-aging profiles depicted in Figure 4, we can interpret the mechanisms of efficiency degradation. The net charge density of the CCWD sample drops from 1.5×10^{14} to $5 \times 10^{13} \text{ cm}^{-3}$ after aging, and similarly the one of the VE-Cu sample, from 2×10^{14} to $4 \times 10^{13} \text{ cm}^{-3}$. More

interesting, for the VE-Cu case, the net charge density measured at lower temperatures (also shown in Figure 4) is low, and the profiles are influenced by back contact effects (ie, the depletion region extends too close to the back contact). As Cu increases, the extension of the depletion region widens to the metal back contact. This trend is stronger with time and can explain the reason of the larger reduction in performance of solar cells contacted with a 2.0-nm-thick Cu layer. A higher amount of copper diffusion from the back contact could lead to the formation of a larger amount of compensating defects. As also suggested by other groups, an excessive copper diffusion can compensate the Cu_{Cd} acceptors with Cu_i donors.^{8,36} Therefore, the smaller amount of Cu needed with the CuCl_2 copper deposition method leads to a reduced formation of compensating defects, and thus to the fabrication of more stable samples.

6 | CONCLUSIONS

A wet deposition method has been developed in order to insert copper at the back contact of CdTe solar cells. Using a solution allows to simply deposit any ideal small amount of copper evenly over the entire area of the sample. In particular, a copper chloride solution has been used because of the well-known effects of chlorine on CdTe such as recrystallization, grain growth,²⁰ and possibly p-type doping.^{20,23}

The samples exhibit a good ohmic back contact without rollover and with efficiencies comparable to those of samples, which are vacuum coated but with an amount of Cu 20 times larger. Moreover, a significant stability improvement has been achieved, as attested by the accelerated aging tests performed at an illumination of one sun and at a temperature of 80°C .

We have detected that the CuCl_2 treatment affects both bulk and back contact of the CdTe.

6.1 | Bulk

CV-DLCP profiles of VE-Cu and CCWD samples reveal the presence of different dominant defects. Only for the CCWD sample the dominant defects, identified by AS, are in a range of energies that have been attributed to the substitutional Cu impurities Cu_{Cd}^- ,^{29,35} known as acceptors in CdTe. Because all the different samples have been CdCl_2 treated, but only CuCl_2 -treated samples show this type of defects, it can be supposed that the introduction of copper bounded to chlorine

helps the solubility of the Cu^-_{Cd} acceptors because chlorine increases their solubility.²⁹ As a consequence, the p-type doping of CdTe is improved.^{8,40} At low temperatures, CV/DLCP show that VE-Cu samples are strongly influenced by back contact effects, their depletion region extends closer to the back contact, and thus the net charge density is low. This effect appears mainly at the lowest temperatures, suggesting the presence of shallow donors, exactly as Cu_i , that, being closer to the band, have faster response at low temperatures than deep defects such as the Cu^-_{Cd} .³³ This effect increases with aging time, due to copper diffusion and consequent formation of Cu_i donors.

6.2 | Back contact

Moreover, TEM images show for CCWD samples a larger inhomogeneity in copper distribution from the back contact to the junction, implying that the copper stays fixed at the back contact.

XPS spectra explain how the copper is fixed: in spite of the reducing copper quantity, the CCWD sample reveals a large presence of Te–Cu peaks, demonstrating that a Cu_xTe compound is formed stabilizing Cu at the back contact.⁹

Compared with VE-Cu, the CCWD process generates more tellurium and less tellurium oxides, which is beneficial to the cell performance as the Te layer is widely used as buffer to reduce the CdTe back contact barrier.⁴⁰ The improved back contact stability, given by the Cu–Te compounds, is supported by the reduced copper diffusion towards the CdTe/CdS junction; this has been confirmed by SIMS depth profiles.

Finally, AST analysis has shown a different degradation of the solar cell devices according to the Cu inclusion method. For VE-Cu solar cells, the degradation in performance is mainly due to the FF reduction. While for the CCWD cells, the degradation is very much limited.

In conclusion, the CuCl_2 wet deposition process is a simple and advantageous method to insert copper in the back contact of CdTe solar cells. It allows the formation of Cu^-_{Cd} acceptor defects, reducing the formation of the compensating donors Cu_i .

In light of the results obtained, the conclusion is that this process step improves the lifetime of CdTe devices, without efficiency losses.

ACKNOWLEDGEMENTS

Prof. Tim D. Veal from the Stephenson Institute for Renewable Energy and Department of Physics at the University of Liverpool (UK) is thankfully acknowledged for the fruitful discussions on the XPS characterization.

ORCID

Alessandro Romeo  <https://orcid.org/0000-0001-5068-8788>

REFERENCES

- Green MA, Hishikawa Y, Dunlop ED, Levi DH, Hohl-Ebinger J, Ho-Bailie AWY. Solar cell efficiency tables (version 52). *Prog Photovolt Res Appl*. 2018;26(7):427-436.
- Philips DS, Warmuth W. Photovoltaics report 2019. *Fraunhofer ISE*, (March), 2019; 1–43.
- Wei SH, Zhang SB. Chemical trends of defect formation and doping limit in II-VI semiconductors: the case of CdTe. *Phys Rev B - Condens Matter Mater Phys*. 2002;66(15):1-10.
- Demtsu SH, Sites JR. Effect of back-contact barrier on thin-film CdTe solar cells. *Thin Solid Films*. 2006;510(1-2):320-324.
- Corwine CR, Pudov AO, Gloeckler M, Demtsu SH, Sites JR. Copper inclusion and migration from the back contact in CdTe solar cells. *Sol Energy Mater Sol Cells*. 2004;82(4):481-489.
- Das SK, Morris GC. Influence of growth and microstructure of electro-deposited cadmium telluride films on the properties of n-CdS/p-CdTe thin-film solar cells. *J Appl Phys*. 1992;72(10):4940-4945.
- Kučys E, Jerhot J, Bertulis K, Bariss V. Copper impurity behaviour in CdTe films. *Phys Status Solidi*. 1980;59(1):91-99.
- Kranz L, Gretener C, Perrenoud J, et al. Doping of polycrystalline CdTe for high-efficiency solar cells on flexible metal foil. *Nat Commun*. 2013;4(1).
- Wu X, Zhou J, Duda a, et al. Phase control of Cu_xTe film and its effects on CdS/CdTe solar cell. *Thin Solid Films*. 2007;515(15):5798-5803.
- Gessert TA, Asher S, Johnston S, Duda A, Young MR, Moriarty T. Formation Of ZnTe: Cu/Ti contacts at high temperature for CdS/CdTe devices. *Conf. Rec. 2006 IEEE 4th World Conf. Photovolt. Energy Conversion*, 2006; 432–435.
- Li J, Diercks DR, Ohno TR, et al. Controlled activation of ZnTe:Cu contacted CdTe solar cells using rapid thermal processing. *Sol Energy Mater Sol Cells*. 2015;133:208-215.
- Romeo N, Bosio A, Mazzamuto S, Romeo A, Vaillant Roca L. High efficiency CdTe/CdS thin film solar cells with a novel back contact. *Proc. 22nd Eur. Photovolt. Sol. Energy Conf.*, 2007; 1919–1921.
- Romeo A, Salavei A, Rimmaudo I, Bosio A, Menossi D, Picinelli F, Romeo N. Electrical characterization and aging of CdTe thin film solar cells with Bi_2Te_3 back contact. *Conf. Rec. 39th IEEE Photovolt. Spec. Conf.*, 2013; 1178–1182.
- Romeo N, Bosio a, Romeo a. An innovative process suitable to produce high-efficiency CdTe/CdS thin-film modules. *Sol Energy Mater Sol Cells*. 2010;94(1):2-7.
- Bätzner DL, Romeo A, Zogg H, Wendt R, Tiwari AN. Development of efficient and stable back contacts on CdTe/CdS solar cells. *Thin Solid Films*. 2001;387(1-2):151-154.
- Greco D, Compaan a D. Photoluminescence study of Cu diffusion and electromigration in CdTe. *Appl Phys Lett*. 1999;75(1999):361-363.
- Dobson KD, Visoly-fisher I, Hodes G, Cahen D. Stability of CdTe/CdS thin-film solar cells. *Sol Energy Mater Sol Cells*. 2000;62(3):295-325.
- Rimmaudo I, Salavei A, Artegiani E, et al. Improved stability of CdTe solar cells by absorber surface etching. *Sol Energy Mater Sol Cells*. 2017;162(December 2016):127-133.
- Gessert TA, Mason AR, Sheldon P, Swartzlander AB, Niles D, Coutts TJ. Development of Cu-doped ZnTe as a back-contact interface layer for thin-film CdS/CdTe solar cells. *J Vac Sci Technol a Vacuum, Surfaces, Film*. 1996;14(3):806-812.
- Dharmadasa I. Review of the CdCl_2 treatment used in CdS/CdTe thin film solar cell development and new evidence towards improved understanding. *CoatingsTech*. 2014;4(2):282-307.
- Major JD, Treharne RE, Phillips LJ, Durose K. A low-cost non-toxic post-growth activation step for CdTe solar cells. *Nature*. 2014;511(7509):334-337.
- Salavei A, Rimmaudo I, Picinelli F, Menossi D, Bosio A, Romeo N, Romeo A. Analysis of CdTe activation treatment with a novel approach. *28th Eur Photovolt Sol Energy Conf Exhib*, 2014; 2140–2142.

23. Castaldini A, Cavallini A, Fraboni B, Fernandez P, Piqueras J. Comparison of electrical and luminescence data for the A center in CdTe. *Appl Phys Lett*. 1996;69(23):3510-3512.
24. Mao D, Blatz G, Wickersham CE, Gloeckler M. Correlative impurity distribution analysis in cadmium telluride (CdTe) thin-film solar cells by ToF-SIMS 2D imaging. *Sol Energy Mater Sol Cells*. 2016;157:65-73.
25. Aris KA, Rahman KS, Enam FMT, Kamaruzzaman MIB, Yahya IB, Amin N. An investigation on copper doping to CdTe absorber layers in CdTe thin film solar cells. 2016 Int Conf Adv Electr Electron Syst Eng, 2016; 405-408.
26. Gordillo G, Grizalez M, Moreno LC, Landazábal F. Influence of the optical window on the performance of TCO/CdS/CdTe solar cells. *Phys Status Solidi Basic Res*. 2000;220(1):215-219.
27. Munshi AH, Kephart JM, Abbas A, et al. Effect of CdCl₂ passivation treatment on microstructure and performance of CdSeTe/CdTe thin-film photovoltaic devices. *Sol Energy Mater Sol Cells*. 2018;186 (June):259-265.
28. Munshi AH, Kephart J, Abbas A, et al. Polycrystalline CdSeTe/CdTe absorber cells with 28 mA/cm² short-circuit current. *IEEE J Photovoltaics*. 2018;8(1):310-314.
29. Beach J, Seymour FH, Kaydanov VI, Ohno TR. Studies of basic electronic properties of CdTe-based solar cells and their evolution during processing and stress. *Subcontract Rep. NREL/SR-520-41097*, (January), 2006.
30. McCandless BE. Thermochemical and kinetic aspects of cadmium telluride solar cell processing. *Proc. 2001 MRS Spring Meet.*, H1.6, 2001; 1-12.
31. Yan Y, Dhere RG, Jones KM, Al-Jassim MM. Influence of substrate structure on the growth of CdTe thin films. *J Appl Phys*. 2001;89(11 I):5944-5948.
32. Bosio A, Romeo A, Menossi D, Mazzamuto S, Romeo N. Review: the second-generation of CdTe and CuInGaSe₂ thin film PV modules. *Cryst Res Technol*. 2011;46(8):857-864.
33. Heath JT, Cohen JD, Shafarman WN. Bulk and metastable defects in CuIn_{1-x}Ga_xSe₂ thin films using drive-level capacitance profiling. *J Appl Phys*. 2004;95(3):1000-1010.
34. Li JV, Halverson AF, Sulima OV, et al. Theoretical analysis of effects of deep level, back contact, and absorber thickness on capacitance-voltage profiling of CdTe thin-film solar cells. *Sol Energy Mater Sol Cells*. 2012;100:126-131.
35. Balcioglu A, Ahrenkiel RK, Hasoon F. Deep-level impurities in CdTe/CdS thin-film solar cells. *J Appl Phys*. 2000;88(12):7175-7178.
36. Tang J, Mao D, Ohno TR, Kaydanov V, Trefny JU. Properties of ZnTe:Cu thin films and CdS/CdTe/ZnTe solar cells. *Proc. 26th IEEE Photovolt. Spec. Conf.*, 1997; 439-442.
37. Rimmaudo I, Salavei A, Romeo A. Effects of activation treatment on the electrical properties of low temperature grown CdTe devices. *Thin Solid Films*. 2013;535:253-256.
38. Wei S-H, Zhang SB, Zunger A. First-principles calculation of band offsets, optical bowings, and defects in CdS, CdSe, CdTe, and their alloys. *J Appl Phys*. 2000;87(2000):1304-1311.
39. Jun-Feng H, Liu X, Li-Mei C, Hamon J, Besland MP. Investigation of oxide layer on CdTe film surface and its effect on the device performance. *Mater Sci Semicond Process*. 2015;40:402-406.
40. Song T, Moore A, Sites JR. Te layer to reduce the CdTe back-contact barrier. *IEEE J Photovoltaics*. 2018;8(1):293-298.

How to cite this article: Artegiani E, Menossi D, Shiel H, et al. Analysis of a novel CuCl₂ back contact process for improved stability in CdTe solar cells. *Prog Photovolt Res Appl*. 2019;27:706-715. <https://doi.org/10.1002/pip.3148>